JBIC Journal of Biological Inorganic Chemistry
https://doi.org/10.1007/s00775-019-01676-z

ORIGINAL PAPER

Green synthesis of copper oxide nanoparticles using sinapic acid: an underpinning step towards antiangiogenic therapy for breast cancer

Desingh Raj Preeth[1] · Manickaraj Shairam[1] · Natarajan Suganya[2] · Roshandel Hootan[3] · Ravishankar Kartik[4] · Kennepohl Pierre[3] · Chatterjee Suvro[2] · Subramaniyam Rajalakshmi[1]

Received: 7 February 2019 / Accepted: 3 June 2019

Abstract

Synthesis of copper oxide nanoparticles without any chemical reductant is always a challenging methodology for biological studies. In this study, sinapic acid, a phytochemical, is used for the synthesis of stable copper oxide nanoparticles. The as-synthesized nanoparticles were characterized thoroughly using UV–Visible, IR spectroscopy, Transmission Electron Microscopy (TEM) and X-ray photoelectron spectroscopy (XPS). Nanoparticles collected during different time intervals of synthesis (60,120 and 180 min) were subjected for analysis, where the occurrence of copper oxide nanoparticles with substantial morphology was seen at 180 min. Further, nanoparticles synthesized at 120 and 180 min were studied for their potential biological applications. These copper oxide nanoparticles evinced potential cytotoxic effects on breast cancer cells, MCF7 and MDA-MB231. Supplementarily, it also exhibited anti-angiogenic effect on endothelial cells (EA.hy926), thus confirming its potential to inhibit angiogenesis in cancer.

Graphic abstract

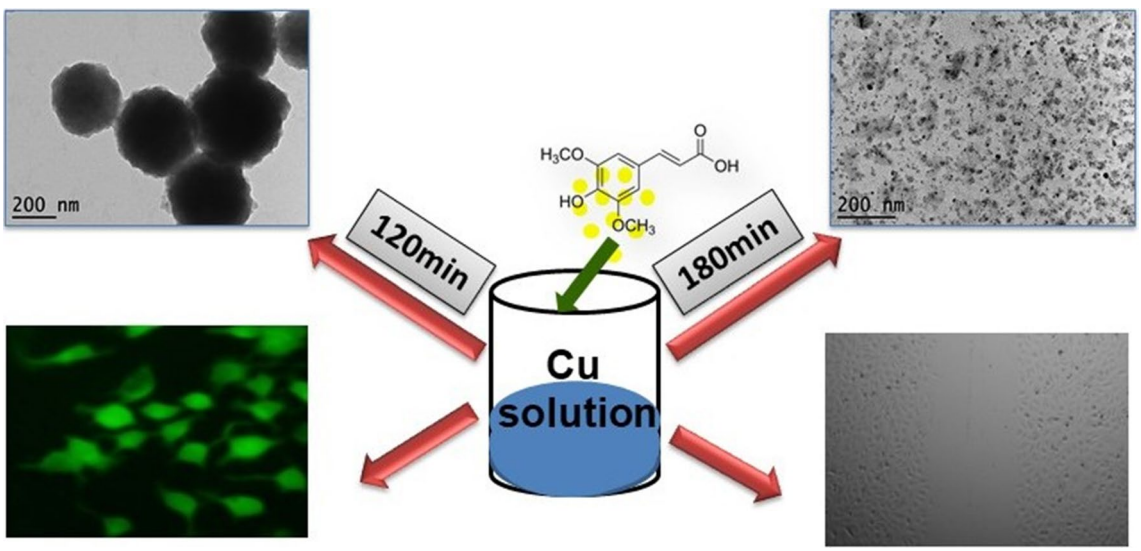

Desingh Raj Preeth and Manickaraj Shairam authors contributed equally.

Electronic supplementary material The online version of this article (https://doi.org/10.1007/s00775-019-01676-z) contains supplementary material, which is available to authorized users.

Extended author information available on the last page of the article

Published online: 22 June 2019

Keywords Angiogenesis · Copper oxide nanoparticle · MCF7 and MDA-MB231 · Sinapic acid · TEM

Introduction

There is a tremendous interest and demand in the past few decades for the easy and cost-effective synthesis of nanoparticles with uniform-size and narrow-size regime [1–4]. There are several methods which have been successfully established including wet chemical synthesis (reduction), chemical vapor deposition, template-assisted synthesis and electronic deposition technologies [5, 6]. Amongst, wet chemical reduction is one of the most feasible ways, since it is versatile in nanostructure control and easy to scale up in low cost. In such methods, metal (II) is reduced using reducing agent (e.g., hydrazine), in an aqueous or non-aqueous medium, in the presence or absence of a surfactant or a capping agent [7, 8]. Metal nanoparticles are being increasingly used in diverse myriad applications because of their enhanced biological and environmental safety compared to other materials [9]. Among metal nanoparticles, Gold, Silver and Copper (coinage metals) nanoparticles have emerged as an important tool for diverse applications, due to their potential need in biomedical, catalysis, photovoltaic and opto-electronic fields [10–12]. Copper nanomaterials including nanowires (CuNWs) and nanoparticles (CuNPs) have received significant attention due to their excellent optical, electrical, catalytic, and antifungal properties [13–15]. And also due to their successive implementations in the fields of catalysis, opto-electronics, chemical sensors, biomedicine and biotechnology [16–18]. There are several methods such as chemical, physical and biological synthetic ways used to produce nanoparticle. With all these mentioned, the chemical synthesis method is the easy to synthesis, cost effective and less time consuming. In the chemical synthetic route, a reductant is used for reducing metal precursor to metal/metal oxide nanoparticle [19]. Therefore, our focus was on the synthesis of metal nanoparticles without addition of any harsh chemical reductants or stabilizing agents [20, 21]. Literature reports the use of hydroxyls where sinapic acid has more interesting biological properties. Sinapic acid (3,5-dimethoxy-4-hydroxycinnamic acid) belongs to phenylpropanoid family and is a naturally available derivative of cinnamic acid. With the antioxidant nature of sinapic acid, it has also been reported for its wide range of effects against metabolic disorders, lung fibrosis, hypertension, cardiovascular dysfunction, ischemia/reperfusion injury [22–25]. In addition, sinapic acid has been evidenced for its anticancer activity against prostate and colon cancer cells [26, 27]. In this connection, with its extensive applications, here we attempted to synthesis the copper oxide nanoparticles with sinapic acid as stabilizing agent and we aimed to explore the anticancer effect of CuONPs against breast cancer cells, in vitro.

As the cancer pathophysiology is concerned, angiogenesis plays a foremost role in the tumor growth and metastasis, especially cancer cells are in need of the vascularisation for further growth of cells beyond 1–2 mm^3 [28]. Angiogenesis is a complex physiological process through which the new blood vessels form from the existing vasculature [29]; hence, many research aimed in the suppression of this angiogenesis which could be one of the most potential anticancer therapies. Currently available anti-angiogenic therapy with chemotherapeutic drugs have been reported for several limitations [30]; hence, targeted execution of cancer cells using nanoparticles has gained a huge importance. In this connection, here we elucidated the anti-angiogenic property of CuONPs (synthesized through green synthetic methodology), in the immortalized endothelial cells (EA.hy926).

Experimental

Materials

Copper(II) sulfate pentahydrate ($CuSO_4.5H_2O$), Sinapic Acid (SA), Sodium borohydride ($NaBH_4$), Thiazolyl Blue Tetrazolium Bromide were purchased from Sigma–Aldrich, India. HPLC grade water was purchased from Merck, India. Biological reagents used for cell culture experiments such as Dulbecco's modified Eagle's medium (DMEM with 4.5 g L^{-1} glucose, 4.0 mM L-glutamine and sodium pyruvate), Penicillin/Streptomycin (10,000 U mL^{-1}), fetal bovine serum (FBS), 0.25% Trypsin–EDTA (1X), Phosphate buffer saline pH 7.4 (PBS) were purchased from Gibco, India.

Synthesis of copper oxide nanoparticle

Copper oxide nanoparticles were synthesized by chemical reduction of copper salt with sinapic acid in alkaline solution. To synthesis copper oxide nanoparticles, initially, copper sulfate (10 mL of 20 mmol) was dissolved in water. To this solution, alkaline solution of sinapic acid (SA) (10 mL of 20 mmol) was added in a drop-wise manner. Immediately, following the addition of alkaline solution of SA, color of the solution turned into turbid yellow from pale blue copper solution. The turbid yellow copper solution was allowed to stir at room temperature for 4 h, where we observed color changes with respect to time. A quick color change was observed from pale blue to turbid yellow and then to brick-red within 30 min. Meanwhile, the reddish Cu nanoparticles started to generate and float in the upper layer of the reaction mixture. After 180 min, the resulting suspension was carefully centrifuged at 10,000 rpm for 10 min. The

resultant nanoparticles obtained was washed with a large amount of deionized water and consequently centrifuged thrice at 10,000 rpm for 10 min. Finally, the nanoparticles were dried in a vacuum concentrator, affording copper oxide nanoparticles.

UV–Visible absorption spectroscopy

Optical absorption spectra of the synthesized nanoparticles were recorded using a UV–Visible spectrophotometer (Jasco, J-710, Japan) and all measurements were performed in 10-mm path-length quartz cuvettes.

Fourier transform infrared (FTIR) spectra

All infrared spectra were characterized using a Vertex 80 V vacuum FT-IR spectrometer (Bruker) to study the vibrational features of the compounds. A pellet was prepared using 2 mg of the dried sample powder and about 300 mg of potassium bromide through hydraulic pressure. [31] In each spectrum, 64 scans between 4000 and 400 cm^{-1} were recorded at a resolution rate of 4 cm^{-1}.

DLS and zeta potential

The size distribution and zeta potential value of the synthesized CuO nanoparticle were analyzed by dynamic light scattering (DLS) and zeta potential (Dip cell) measurement using a Malvern Zetasizer Nano ZS instrument (Malvern Instruments, Malvern, UK). Diluted dispersed solution of synthesized nanoparticle was prepared in Milli-q-water and sonicated for 30 min at room temperature. Samples were measured in glass cuvettes at 25 °C with detection scattering angle 90^0, each measurement took a 30-s equilibration time. Each sample was analyzed three times per analysis run and each sample was replicated independently three times to analyze particle size, polydispersity and Zeta potential value.

Transmission electron microscopy (TEM)

Transmission electron microscopy (TEM, Hitachi, H-7650, Japan) images were recorded to observe the constitutive nanoparticles using a Philips at an accelerating voltage of 200 kV. For making TEM observations, the sample was suspended in aqueous solution under ultrasonic treatment prior to direct deposition on a copper grid and air-drying.

X-ray photoelectron spectroscopy

X-ray photoelectron spectra were obtained using a Leybold MAX200 with monochromatized Al Kα X-ray source (1486 eV, 20 mA). Survey scans were measured with pass energy of 192 eV and 48 eV for narrow scans. Spectra were energy corrected with respect to the adventitious C 1 s peak at 285.0 eV. Line fitting technique was used to analyze the Cu 2p peaks using XPS Fit software and Microsoft Excel. Reference data regarding Cu 2p peaks and Cu LMM (Auger) peaks were obtained from the La Trobe University XPS database [32] and Mark C. Biesinger's Copper XPS data. [33].

Cell and culture conditions

The immortalized breast cancer cell lines, MCF7 and MDA-MB231 were obtained from the National Center for Cell Sciences (NCCS), Pune, India. The immortalized endothelial hybrid cell line, EA.hy926 was obtained as a kind gift from Dr. C.J.S. Edgell, University of North Carolina, Chapel Hill. The cells were cultured in DMEM medium supplemented with 10% FBS (*v/v*) and 1% penicillin/streptomycin (*w/v*). The cells were maintained at 37 °C in a humidified 5% CO_2 incubator.

Cytotoxicity and cell morphology

MCF7, MDA-MB231 and EA.hy926 cells were seeded at 1×10^4 cells/well in 96-well plates and treated with different concentrations (1,5,10,17,25,37,50,100 µg mL^{-1}) of CuONPs 120 and 180 min, CuONPs synthesized by chemical reduction method ($NaBH_4$), controls (SA, $CuSO_4.5H_2O$) and were incubated for 24 and 48 h. At the end of the experimental period, the treated medium was removed and the cells were washed with PBS and imaged for cell morphology. The cytotoxicity was measured using MTT assay, wherein after the treatment, 10-µL MTT solution (5 mg/ml) was added to 100 µL of the growth medium without phenol red and plates were incubated at 37 °C for 4 h in a humidified 5% CO_2 atmosphere. Then, formazan crystals formed by mitochondrial reduction of MTT were solubilized in dimethyl sulfoxide (100 µL/well) and absorbance was read at 540 nm using a microplate reader. Percentage inhibition of cytotoxicity was expressed as percentage of cell viability compared with control cells.

Intracellular ROS assay

Intracellular ROS was measured using oxidation-sensitive dye, 2,7-dichloro-dihydro-fluorescin diacetate (DCFH-DA). MCF7 and MDA-MB231 cells of 40% confluent were seeded on 24-well plate cover slips. Cells were treated with respective concentrations of CuO NPs. After 24 h of treatment, the cells were incubated with DCFH-DA for 15 min at 37 °C. The cells were washed with 1X PBS and imaged using Olympus IX71 inverted fluorescence microscope and fluorescence intensity was calculated. The fluorescence

intensity was directly proportional to the free radicals produced by the cells.

Endothelial cell wound healing assay

EA.hy926 cells were seeded as a monolayer of 100% confluence at the day of experiment and scratch wound was made using sterile tip and the cells were subjected to different concentration of CuONPs (both 120 and 180 min) and observed for 6 h. For every 2-h interval, images were taken using Olympus IX71 epifluorescence microscopy (4X magnification). Images were processed using Image J software and the wound area was measured.

Statistical analysis

All the experiments were performed in triplicates ($n=3$) and the data are presented as mean ± SD. One-way ANOVA, student *t* test and Turkey post hoc tests were used to analyze the data. SigmaStat software package 6.0 was used for all statistical analysis and calculation of SD values. p values ≤ 0.05 was considered as statistically significant.

Result and discussion

Synthesis and characterization

Copper oxide nanoparticles were synthesized by the use of SA in aqueous medium. The as-synthesized nanoparticles were characterized by UV–Visible and FTIR spectroscopic methods. The UV absorption spectrum of SA showed that characteristic peaks at 227 and 306 nm correspond to π–π* and n–π* transitions, respectively. When SA started to react with copper solution at room temperature, the absorption spectra of the SA shifted from 227 to 244 nm and from 306 to 347 nm (Fig. 1). These shifts in wavelength indicate the involvement of sinapic acid in the nanoparticle formation. Moreover, with respect to time (from 0 to 180 min), we observed a gradual increase in the intensity of absorption band around 350 nm. The color of the solution underwent visible changes from yellow to red and finally to reddish brown till 180 min. This is an interesting parameter to characterize the formation of nanoparticle because the reddish-brown coloration showed the formation of copper oxide nanoparticles. [34, 35] Thereafter, the absorption band lowered considerably with time accompanying the color changes from reddish brown to clear brown.

To characterize the as-synthesized nanoparticle, the functional group analyses were performed using FTIR spectroscopy. The characteristic sinapic acid bands were seen at 3382 cm^{-1} corresponds to hydroxyl group, 2298 cm^{-1} corresponds to phenolic groups and 1650 cm^{-1} indicating carbonyl stretching frequencies. The formation of nanoparticles after the addition of SA was confirmed by the absence of 3382 cm^{-1}(−OH) stretching frequency which represents the involvement of hydroxyl group. Besides, the carbonyl stretching frequency of sinapic acid was red shifted by 50 cm^{-1} (1650–1700) which clearly depicts that the carbonyl (C = O) and hydroxyl (−OH) groups in SA [36] were involved in the formation of nanoparticles, which is seen from the Fig. 2 (a, b). With respect to different time intervals, these IR bands have not shown much difference. In the aqueous dispersed solution of synthesized CuO nanoparticle, the particle size and zeta potential value of 120 and 180 min samples were found to be 250 nm and − 26 mV, 40 nm and − 28 mV, respectively. The PDI values 0.3 and 0.2 for 120 and 180 min, respectively, indicated an even size distribution of the synthesized CuO nanoparticles. [37] The more negative zeta potential values indicated stability of the synthesized nanoparticle. [38] These results conclude that the synthesized CuO nanoparticle was monodispersed and stable in nature. TEM helps to understand the size of the formed nanoparticles. The formation of nanoparticles with respect to time was also been studied. From the TEM image at 0th min (Figure S1), we could see that the nanoparticles formation was feasible, immediately after the addition of alkaline solution of SA into the Cu(II) solution (pale blue color). But the so-formed nanoparticles were not well defined till 60 min where we could see the excess sinapic acid in the matrix through electron microscopy. It was also seen from the visible changes of the reaction mixture from pale blue to blood red in color. As the time proceeds, the color of the

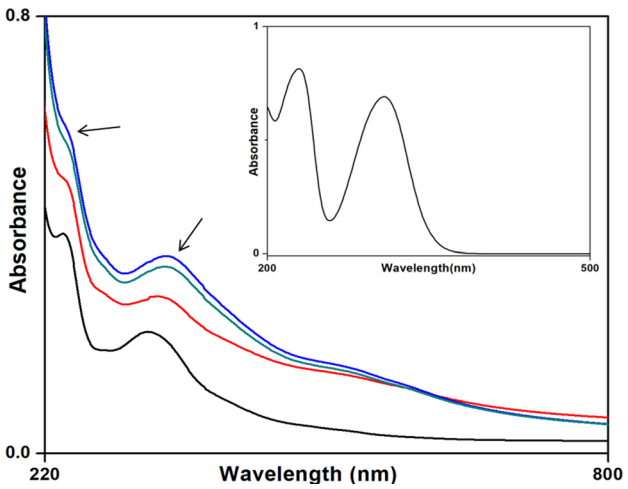

Fig. 1 Corresponding UV–Visible spectra of Copper oxide nanoparticle (black: 0 min; red: 60 min; aqua: 120 min blue: 180 min) at different time intervals. Inset: UV visible spectra of sinapic acid. The image indicates the final color of the formed CuO nanoparticles

reaction mixture was completely turned into brown solution. At 30 (Fig. 3a) and 60 min (Fig. 3b), we observed the formation of nanoparticle > 200 nm with not well-defined morphology, which was evident from the images. On the other hand, a well-defined morphology with distinct particle size was clearly seen at 120 min (Fig. 3c). As seen in the figure, the spherical-shaped nanoparticles were formed but whose particle size was > 200 nm. So, the reaction was further proceeded till 180 min, where the color of the solution became intense brown. The respective TEM image is shown in the Fig. 3d, which indicated that the size of the particles was below 20 nm. To further analyze the fine size of the as-synthesized nanoparticles, a higher magnification was used where the size was almost 10 nm with spherical morphology which was clearly seen from Fig. 4a. Therefore, for further analysis and biological studies CuO NPs synthesized at 120 and 180 min were chosen due to their fine size and morphology. The SAED pattern of synthesized CuO NPs is shown in the Fig. 4b. It was observed that planes [(111), (200), (220)], [(002), (200)] and [(220) (111)] from bright circular rings showed that the synthesized nanoparticle contains phases of CuO and also Cu_2O [39–42].

Figure 5 shows the XPS survey spectra of CuO NPs synthesized at 180 min. All the indexed peaks correspond to copper (Cu), carbon (C) and oxygen (O). The two shakeup satellite peaks for Cu 2p3/2 (934.7 eV) and Cu 2p1/2 (955.3 eV) are indicative of a d^9 transition metal, i.e., Cu^{2+} [39, 43]. The gap between the two (Cu $2p_{3/2}$ and Cu $2p_{1/2}$) is 20.6 eV, which is in agreement with the standard value of 20.0 eV for CuO [44, 45]. But, the asymmetry and broadness of the main Cu 2p peaks suggest the presence of more than one form of copper in the sample. Detecting and distinguishing other copper forms (Cu^0 and Cu^{1+}) are difficult due to their spectral overlap in the Cu 2p region with Cu^{2+}. Copper Auger peaks provide the necessary information required to determine and distinguish the two copper forms. Cu (0) and Cu (1 +) have distinct spectral patterns in the Cu LMM region. Although Cu^{2+} makes detection of these distinct patterns difficult, the shoulder peaks of Cu (0) were visible. Characterization of NPs reveals the presence of Cu^{2+} being the dominant form. The observed Cu^{2+} signals are consistent with the presence of CuO NPs.

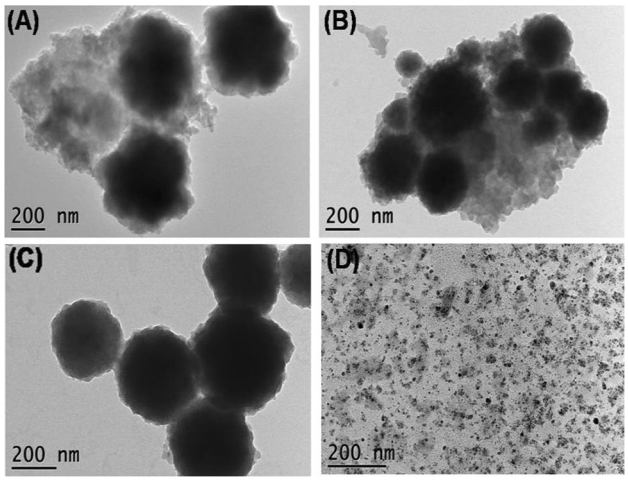

Fig. 3 TEM image of Copper oxide nanoparticle from the dried samples of **a** 30 min **b** 60 min **c** 120 min **d** 180 min. (Scale bar: 200 nm)

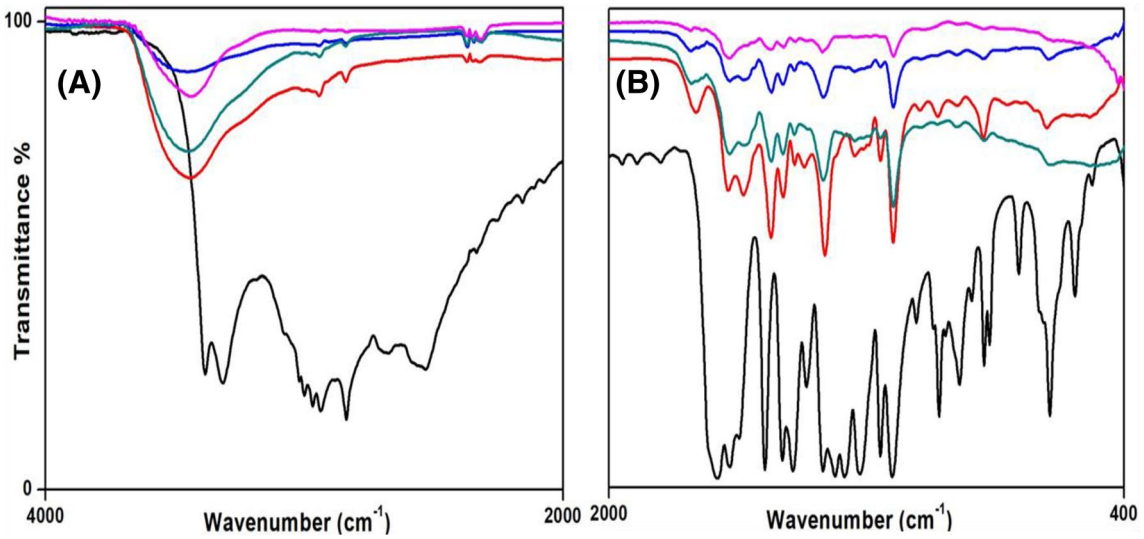

Fig. 2 **a**, **b**: FTIR spectra of synthesized copper oxide nanoparticle SA alone(black); CuONP at 30 min (red), CuONP at 60 min (aqua), CuONP at 120 min (blue), CuONP at 180 min (pink)

Anticancer activity

Copper-based compounds have received huge biological impact in the past two decades and being one of the most important biological trace elements, copper plays a tremendous role as anticancer agents [46, 47]. On the other hand, role of polyphenolic compound, sinapic acid, has also been reported for its anticancer mechanism [26, 27]. Most challenging concern in the use of polyphenols as chemo-preventive agent is due to low oral bioavailability [48]. To overcome this problem, nanonization is the prominent approach emerging recently and it is also inclined to be the targeted approach against the cancer cells growth. In the current study, the cytotoxic effect of synthesized CuO NPs, at both 120 and 180 min, were subjected to breast cancer cell lines, MCF7 and MDA-MB231 and investigated for their potential activities. We have chosen breast cancer cell lines, MCF7 and MDA-MB231 due to their well-documented studies and different characteristics as reported by Moses et al. 2016 [49]. In particular, MCF7 cells have been recognized most and used in the breast cancer research because of its acute hormone sensitivity owing to the expression of estrogen receptor, which makes it as an ideal model to study hormone response [50]. Meanwhile, MDA-MB231 cells are known for the gene expression linked with specific metastatic sites and are the triple-negative breast cancer cells which are the aggressive cancers, which are not controlled by hormonal therapy [51, 52].

Initially, we checked the cytotoxicity of SA control in both MCF7 and MDA-MB231 cells, and it did not show any cytotoxic effect at concentrations up to 100 µg mL^{-1} at 24 and 48 h (Figure S2 A and B). It has been reported by Eroğlu et al., that SA at higher concentration of 1000 µM induced cytotoxic effect against human prostate cancer cells [26]. In MCF7 cells, the IC_{50} value for

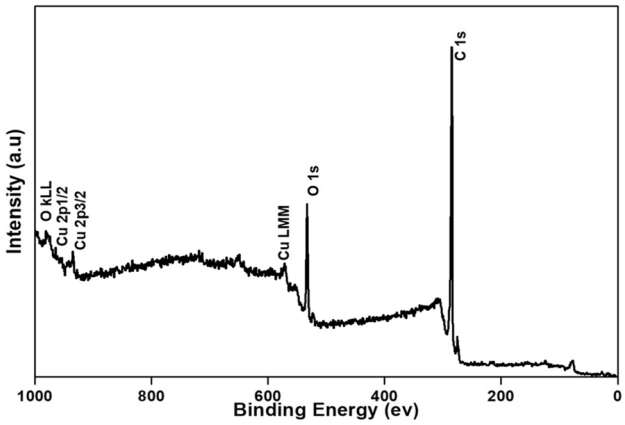

Fig. 5 XPS survey spectra of Copper oxide nanoparticle from the dried Samples of 180 min

CuO NPs 120 min at 24 and 48 h was found to be 21.5 and 15 µg mL^{-1}, respectively. Moreover, for CuO NPs 180 min, IC_{50} was observed to be 24.5 and 14 µg mL^{-1} at 24 and 48 h, respectively (Fig. 6a, b) and the cytotoxicity increases with concentration and in a time-dependent manner when compared to control cells. In addition, with MDA-MB231 cells, the IC_{50} value for CuO NPs 120 min at 24 and 48 h was found to be 7.5 and 6.5 µg mL^{-1}, respectively. For CuO NPs at 180 min, IC_{50} was observed to be 11 and 9 µg mL^{-1} at 24 and 48 h, respectively, and dose-dependent increase in cell death was also observed (Fig. 6c, d). Together with the growth inhibition, the results displayed distinct changes in the morphology of both MCF7 and MDA-MB231 cells towards CuO NPs treatment with increase in concentration (Figure S3 A and B). Moreover, comparably CuO NPs 120 min showed more lethal effect on cancer cells when compared to 180 min at IC_{50} concentration. The earlier evidences have pointed

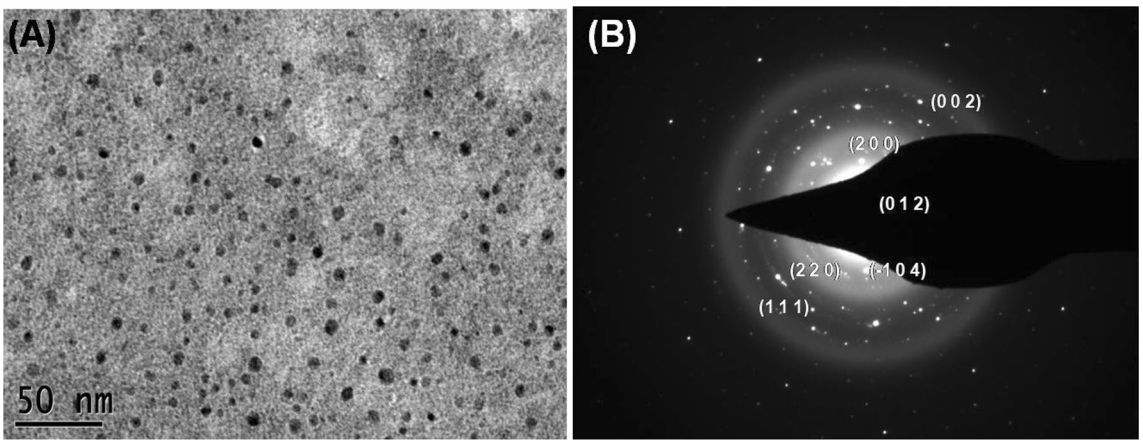

Fig. 4 **a** TEM image of Copper oxide nanoparticle from the dried Samples of 180 min **b** selected area electron diffraction pattern of copper oxide nanoparticle (scale bar: 10 nm^{-1})

out that the copper in the nanoparticles form showed anticancer activity against various cell types including breast cancer [53, 54] The current study highlights the exploitation of the polyphenol–metal nanoparticle as the chemopreventive agent against breast cancer. The CuO NPs showed enhanced toxic effect at both time intervals when compared to that of sinapic acid alone. The enhanced cytotoxicity observed at much lower concentrations such as 21.5 and 7.5 µg mL^{-1} for MCF7 and MDA-MB231, respectively, confirmed that formation of sinapic acid-assisted copper oxide nanoparticles is more effective when compared to that of sinapic acid. As polyphenols are considered for anticancer treatment, higher doses needed to overcome its short half lives, improving the bioavailability. On the other hand, the advantage of using nanoparticles is to improve the efficacy with lower dosage [26], hence this study employed SA which acts as both reducing and stabilizing agent for the copper oxide nanoparticles. Therefore, CuO NPs synthesized using sinapic acid showed toxic effect at very low concentrations against breast cancer cell lines. Copper oxide nanoparticles were also synthesized by chemical reduction method and the control experiments along with copper salt were also subjected towards breast cancer cell lines and the results are shown in ESM_1.

As the mechanistic point of view, the cancer cells display an elevated level of oxidative stress with increase in the production of reactive oxygen species (ROS). However, to compensate the ROS, the cancer cells maintain the delicate balance of antioxidant enzymes. [55] Evidences suggest that the cancer cells are vulnerable to abnormal increase in the level of ROS insults and it can be exploited for the targeted exhaustion of the cancer cells. Hence, modulation in the intracellular ROS levels has been considered as the promising anticancer activity and evidence demonstrated the use of novel ROS-modulating agent against cancer cell [56]. Furthermore, nanoparticles have been known to induce cellular toxicity by increasing intracellular ROS levels.

The induction of ROS in the biological system by nanoparticles is known to disrupt the homeostatic redox state and induce cellular genotoxicity, ending up with programmed cell death [57]. In the present study with CuO NPs, we observed the induction of intracellular ROS when assessed using DCF fluorescence. When comparing to the MCF7 cells, the CuO NPs showed cytotoxicity at lower concentrations in MDA-MB231 cells; hence, according to the cytotoxicity observed in the breast cancer cells, we have chosen two different concentrations for ROS detection, a lower and a higher concentration from the IC_{50} values at 24 h, specifically 17 and 25 µg mL^{-1} for MCF7 cells (Fig. 7a, b), and 5 and 10 µg mL^{-1} for MDA-MB231 cells (Fig. 7c, d). The results showed the induction of intracellular ROS in dose-dependent manner in both the cell types; moreover, these

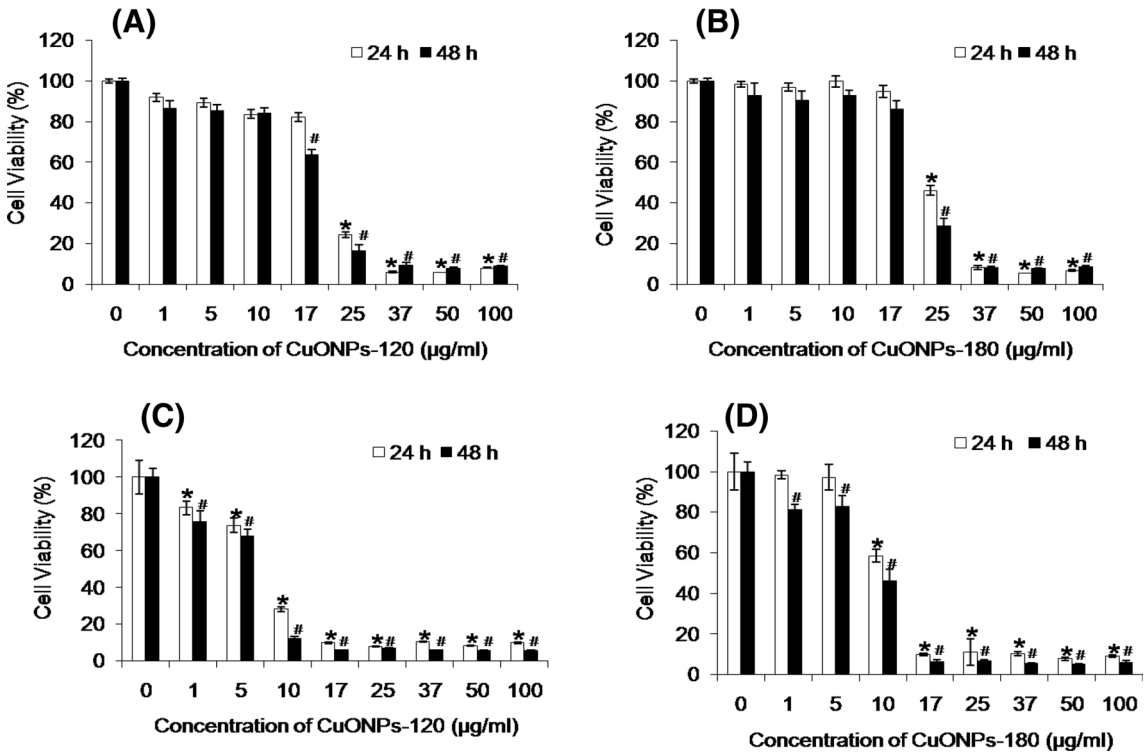

Fig. 6 Effect of **a** CuONPs-120 and **b** − 180 on the cell viability of MCF7 at 24 and 48 h, respectively. Effect of **c** CuONPs-120 and **d** − 180 on the cell viability of MDA-MB231 at 24 and 48 h, respectively. *Considered statistically significant ($p < 0.05$) from control at 24 h and # at 48 h

results correlate with the evidence that copper nanoparticles have been substantiated to induce ROS levels in breast cancer cells like MCF7 [58] and MDA-MB231 [59]. However, the mode of action of the nanoparticles in relation to their chemical properties should be ascertained to reveal the exact mechanism underlying the nanotoxicity. Anticancer activity of CuO NPs are not only attributed by the phenolic groups of sinapic acid present on the surface but also due to their shape, size and other properties of nanoparticles. On the other hand, SA polyphenol control at same concentrations of CuO NPs did not show ROS production (Figure S4).

Anti-angiogenic activity

Currently, anti-angiogenic therapy is one of the feasible therapeutic choices in cancer treatment. Many nanoparticle complexes such as gold, silver, silica-based nanoparticles and others have been reported for their anti-angiogenic activity. [60–63] To unveil the anti-angiogenic property of synthesized CuO NPs, here we exploited the endothelial cell line, EA.hy926. Initially, we checked the cytotoxicity of SA control in EA.hy926 cells and it did not show any cytotoxic effect at concentrations till 100 µg mL^{-1} at 48 h (Figure S2 C). Besides, copper salt and CuONPs synthesized by chemical reduction method were also studied against EA.hy926 and the results are discussed in ESM_1. Furthermore, synthesized CuO nanoparticles (120 and 180 min) were found

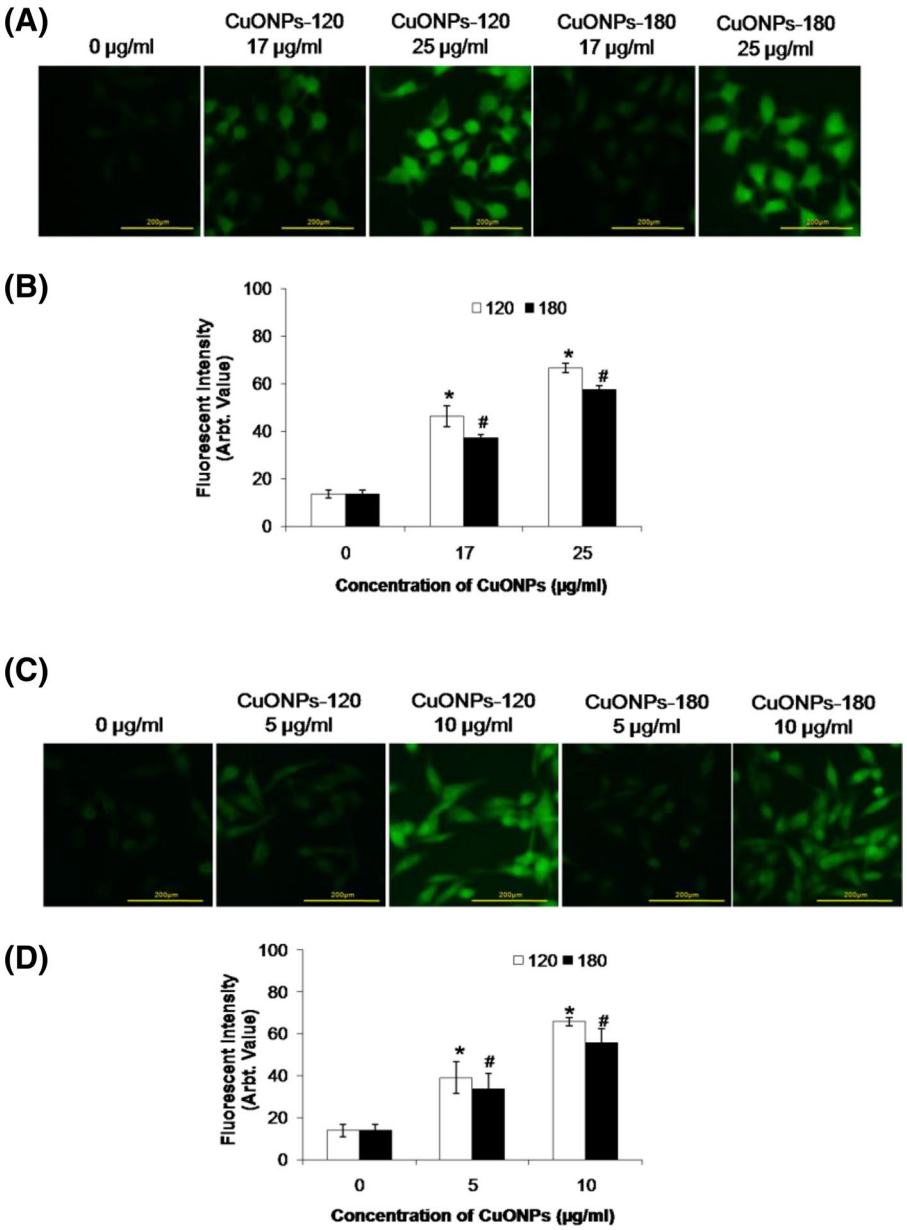

Fig. 7 Induction of intracellular ROS (**a**) and (**c**) in MCF7 and MDA-MB231 cells, respectively, the corresponding representation of fluorescent intensity measurement (**b**) and (**d**) using Image J software. *Considered statistically significant ($p < 0.05$) from control with CuONPs 120 and # with 180

to be non-toxic till 25 μg mL^{-1} and further increase in the concentration to 37 μg mL^{-1} at 24 h showed reduction in cell viability to 55 and 66% for CuO NPs 120 and 180, respectively; whereas further increase in the concentration to 50 and 100 μg mL^{-1} reduced the cell viability completely (Fig. 8A & B). However, CuONPs at lower concentrations showed cytotoxic effect at 48 h, in which concentration from 25 μg mL^{-1} showed pronounced effects. Our results confirms antiangiogenic potential of synthesized nanoparticles through the inhibition of endothelial cell proliferation in dose- and time-dependent manner, which coincides with the study of Song et al. [64].

Endothelial cell migration is an essential part of angiogenesis and an obligatory mechanism for the cancer cell growth and metastasis. [65] Hence, we checked the anti-migration ability of CuO NPs on endothelial cells, by scratch wound healing assay. At low concentration of CuO NPs at 120 and 180 (5 and 10 μg mL^{-1}), a statistically insignificant wound healing was observed when compared to control cells. On the other hand, with increase in the concentrations (both CuO NPs 120 and 180) 17, 25 and 37 μg mL^{-1}, there was a decrease in the wound healing capacity when compared to control in a time-dependent manner (Fig. 9a, b, c). Trickler et al. [66] explained the effect of copper nanoparticles in rat cerebral micro-vessel endothelial cells and evidenced that the Cu-NPs at low concentrations increased cellular proliferation promoting neovascularization and wound healing, where in the reverse effect at higher concentration, which requires further investigation with our synthesized CuO NPs. The migration of endothelial cells was significantly inhibited in the presence of the CuO NPs at higher concentrations, which showed its more pronounced effects on cell motility (Figure S5). This result affirms that synthesized copper oxide nanoparticle exhibits anti-angiogenic activity which correlates with the work of Zheng et al., stating that the nanoparticles significantly blocks the endothelial cell migration and thereby inhibits the angiogenesis [67]. SA did not show any significant effect on cell migration in the wound healing assay (up to 37 μg mL^{-1} in comparison with synthesized CuONPs) similar to that of untreated control (Figure S6). On the other hand, SA-assisted CuO NPs showed significant reduction in the wound healing activity, which further confirms the potential effect of nanoparticles against cancer treatments.

From our present preliminary studies, we confirm that copper oxide nanoparticles synthesized using sinapic acid could be used in the treatment for the breast cancer in which pathological angiogenesis plays a significant role in the tumor growth.

Conclusion

The results from this study unveil the anticancer activity of the CuO NPs synthesized using sinapic acid. The green synthesized CuO NPs were stable and its anticancer activity could be attributed through increase in ROS generation and its ensuing action on inhibiting cell proliferation. In addition, it is reasonable to understand the anti-angiogenesis properties of newly synthesized CuO NPs which could be the reason for its anticancer activity against breast cancer cells. Although, the current findings affirm the effect of synthesized CuONPs for its antiangiogenic effect and we found that the results necessitate further mechanistic confirmation in signaling point of view. When comparing to the native sinapic acid polyphenol, the synthesized

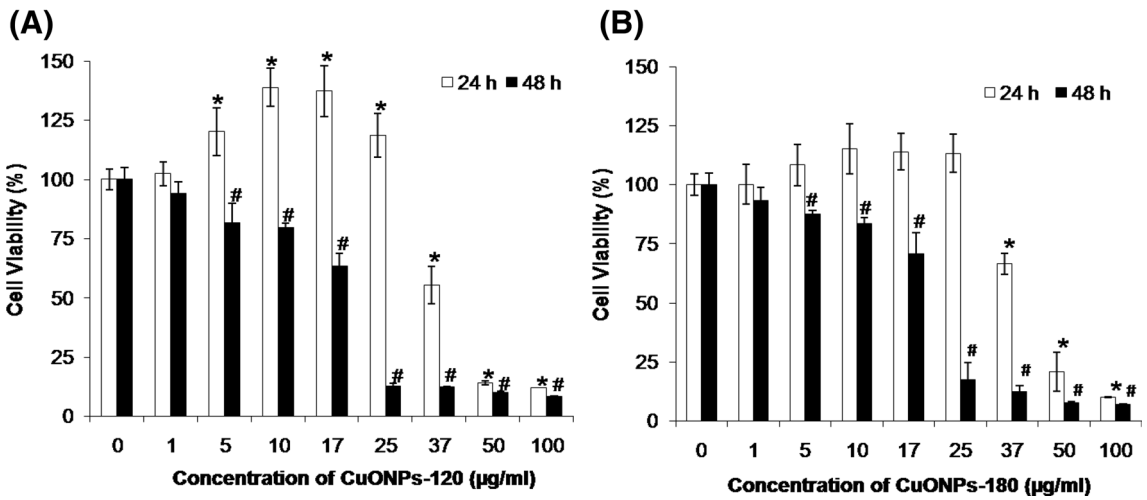

Fig. 8 Effect of **a** CuONPs-120 and **b** – 180 on the cell viability of EA.hy926 at 24 and 48 h. *Considered statistically significant ($p < 0.05$) from control at 24 h and # at 48 h

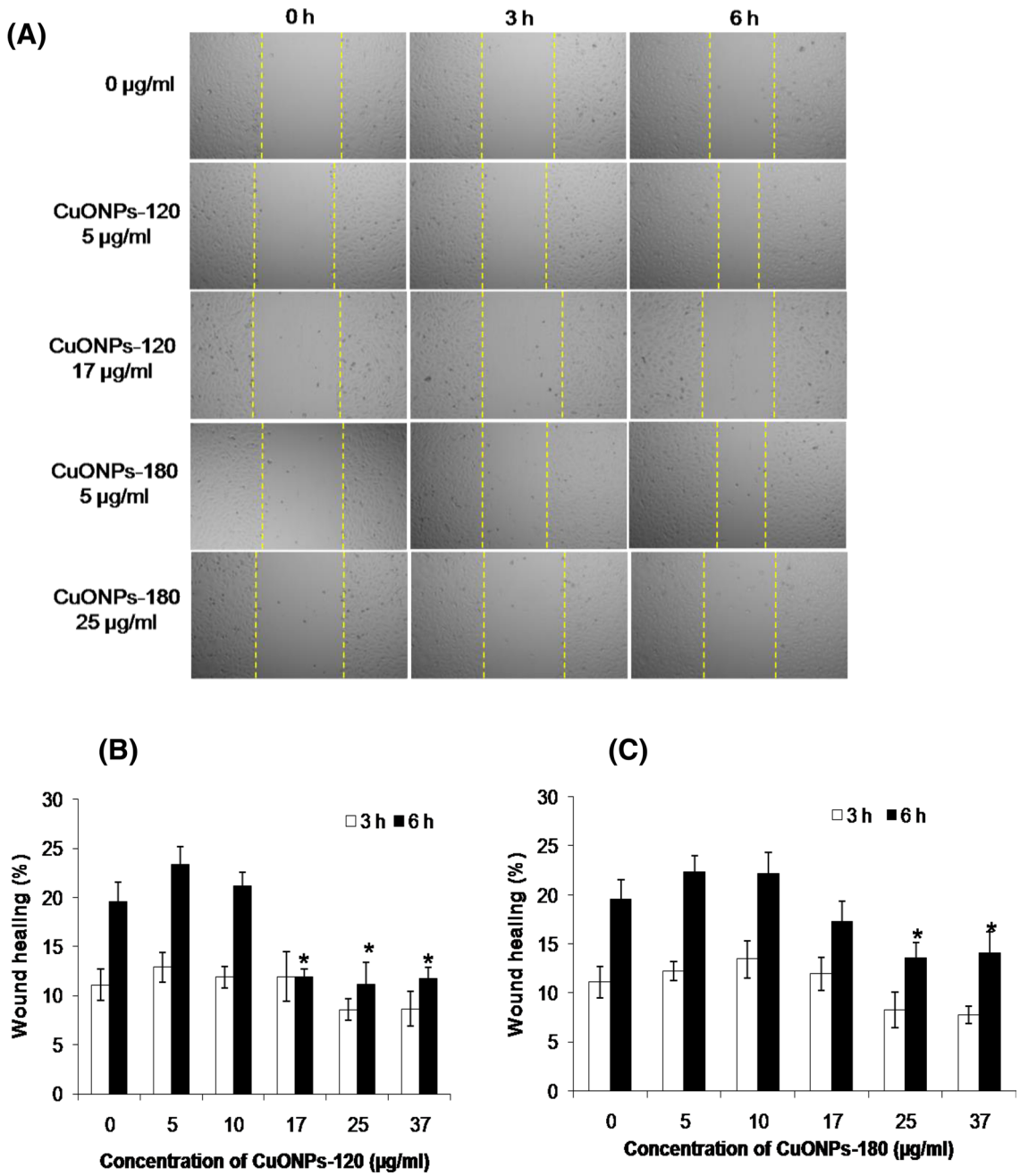

Fig. 9 (**a** Bright field images of scratch wound assay at 0, 3 and 6th h, **b**, **c** the corresponding wound healing in % when compared to the control. *Considered statistically significant ($p < 0.05$) from respective controls of CuONPs 120 and 180

nanoparticles offered a promising effect at its low concentration and could probably be a potential candidate in cancer treatment.

Acknowledgements Dr. S. Rajalakshmi wishes to thank DST-Inspire Faculty (Grant No. DST/INSPIRE/04/2015/001945) program for the research grant. XPS spectra were acquired by Dr. Ken Wong from Advanced Materials and Process Engineering Lab (AMPEL) at University of British Columbia.

Compliance with ethical standards

Conflict of interest There are no conflicts to declare.

References

1. Ben Aissa MA, Tremblay B, Andrieux-Ledier A, Maisonhaute E, Raouafi N, Courty A (2015) Copper nanoparticles of

well-controlled size and shape: a new advance in synthesis and self-organization. Nanoscale 7(7):3189–3195
2. Alzahrani E, Ahmed RA (2016) synthesis of copper nanoparticles with various sizes and shapes: application as a superior non-enzymatic sensor and antibacterial agent. In J Electrochem Sci 11(6):4712–4723
3. Mott D, Galkowski J, Wang L, Luo J, Zhong CJ (2007) Synthesis of size-controlled and shaped copper nanoparticles. Langmuir 23(10):5740–5745
4. Pan K, Ming H, Yu H, Liu Y, Kang Z, Zhang H, Lee ST (2011) Different copper oxide nanostructures: Synthesis, characterization, and application for C-N cross-coupling catalysis. Crys Res Technol 46:1167–1174
5. Biswas A, Bayer IS, Biris AS, Wang T, Dervishi E, Faupel F (2012) Advances in top-down and bottom-up surface nanofabrication: techniques, applications & future prospects. Adv Coll Interface Sci 170(1–2):2–27
6. Dang TM, Le TT, Fribourg-Blanc E, Dang MC (2011) The influence of solvents and surfactants on the preparation of copper nanoparticles by a chemical reduction method. Adv Nat Sci Nanosci Nanotechnol 2(2):025004
7. Saikova SV, Vorob'ev SA, Nikolaeva RB, Mikhlin YL (2010) Conditions for the formation of copper nanoparticles by reduction of copper (II) ions with hydrazine hydrate solutions. Russ J Gen Chem 80(6):1122–1127
8. Jin-Cheng Yu, Zhao Fu-Gang, Shao Wei, Geb Cong-Wu, Li Wei-Shi (2015) Shape-controllable and versatile synthesis of copper nanocrystals with amino acids as capping agents. Nanoscale 7:8811–8818
9. Zhongying W, Von Annette Dem B, Kabadi KP, Agnes B, Robert HK (2013) Biological and environmental transformations of copper-based nanomaterials. ACS Nano 7(10):8715–8727
10. Jordan AJ, Lalic G, Sadighi JP (2016) coinage metal hydrides: synthesis, characterization, and reactivity. Chem Rev 116(15):8318–8372
11. Hokita Y, Kanzaki M, Sugiyama T, Arakawa R, Kawasaki H (2015) High-Concentration Synthesis of Sub-10-nm Copper Nanoparticles for Application to Conductive Nanoinks. ACS Appl Mater Interfaces 7:19382–19389
12. Zhou M, Tian M, Li C (2016) Copper-based nanomaterials for cancer imaging and therapy. Bioconjug Chem 5:1188–1199
13. Sabbaghan M, Beheshtian J, Liarjdame RN (2015) Preparation of Cu_2O nanostructures by changing reducing agent and their optical properties. Mater Lett 153:1–4
14. Gawande MB, Goswami A, Felpin FX, Asefa T, Huang X, Silva R, Zou X, Zboril R, Varma RS (2016) Cu and Cu-based nanoparticles: synthesis and applications in catalysis. Chem Rev 116:3722–3811
15. Cioffi N, Torsi L, Ditaranto N, Tantillo G, Ghibelli L, Sabbatini L, Bleve-Zacheo T, D'Alessio M, Zambonin PG, Traversa E (2005) Copper nanoparticle/polymer composites with antifungal and bacteriostatic properties. Chem Mater 17(21):5255–5262
16. Solomon EI, Heppner DE, Johnston EM, Ginsbach JW, Cirera J, Qayyum M, Kieber-Emmons MT, Kjaergaard CH, Hadt RG, Tian L (2014) Copper active sites in biology. Chem Rev 114(7):3659–3853
17. Ingle AP, Duran N, Rai M (2014) Bioactivity, mechanism of action, and cytotoxicity of copper-based nanoparticles: a review. Appl Microbiol Biotechnol 98(3):1001–1009
18. Jaydeep B, Utpal C, Omprakash S, Prasenjit S, Anjan KD (2006) Interaction of hemoglobin and copper nanoparticles: implications in hemoglobinopathy. Nanomedicine 2(2):191–199
19. Gonçalves RV, Wojcieszak R, Wender H, Dias SBC, Vono LL, Eberhardt D, Teixeira SR, Rossi LM (2015) Easy access to metallic copper nanoparticles with high activity and stability for CO oxidation. ACS Appl Mater Interfaces 7(15):7987–7994
20. Mahmoud N, Mohammad S, Mehdi K (2014) Green synthesis of copper nanoparticles using aqueous extract of the leaves of Euphorbia esula L and their catalytic activity for ligand-free Ullmann-coupling reaction and reduction of 4-nitrophenol. RSC Adv 4:47313–47318
21. Jing X, Ye W, Qunji X, Xuedong W (2011) Synthesis of highly stable dispersions of nanosized copper particles using L-ascorbic acid. Green Chem 13:900–904
22. Chen C (2016) sinapic acid and its derivatives as medicine in oxidative stress-induced diseases and aging. Oxid Med Cell Longev 2016:3571614
23. Zych M, Kaczmarczyk-Sedlak I, Wojnar W, Folwarczna J (2018) The effects of sinapic acid on the development of metabolic disorders induced by estrogen deficiency in rats. Oxid Med Cell Longev 2018:9274246
24. Raish M, Ahmad A, Ansari MA, Ahad A, Al-Jenoobi FI, Al-Mohizea AM, Khan A, Ali N (2018) Sinapic acid ameliorates bleomycin-induced lung fibrosis in rats. Biomed Pharmacother 108:224–231
25. Silambarasan T, Manivannan J, Raja B, Chatterjee S (2016) Prevention of cardiac dysfunction, kidney fibrosis and lipid metabolic alterations in l-NAME hypertensive rats by sinapic acid–Role of HMG-CoA reductase. Eur J Pharmacol 777:113–123
26. Eroğlu C, Avcı E, Vural H, Kurar E (2018) Anticancer mechanism of Sinapic acid in PC-3 and LNCaP human prostate cancer cell lines. Gene S0378–1119(18):30539
27. Balaji C, Muthukumaran J, Nalini N (2014) Hemopreventive effect of sinapic acid on 1,2-dimethylhydrazine-induced experimental rat coloncarcinogenesis. Hum Exp Toxicol 33(12):1253–1268
28. Caporarello N, Lupo G, Olivieri M, Cristaldi M, Cambria MT, Salmeri M, Anfuso CD (2017) Classical VEGF, notch and Ang signalling in cancer angiogenesis, alternative approaches and future directions. Mol Med Rep 16(4):4393–4402
29. Carmeliet P (2005) Angiogenesis in life, disease and medicine. Nature 438(7070):932–936
30. Lupo G, Caporarello N, Olivieri M, Cristaldi M, Motta C, Bramanti V, Avola R, Salmeri M, Nicoletti F, Anfuso CD (2016) Anti-angiogenic therapy in cancer: downsides and new pivots for precision medicine. Front Pharmacol 7:519
31. Rajalakshmi S, Vimalraj S, Saravanan S, Preeth DR, Shairam M, Anuradha D (2018) Synthesis and characterization of silibinin/phenanthroline/neocuproine copper (II) complexes for augmenting bone tissue regeneration: an in vitro analysis. J Biol Inorg Chem 19:1
32. Barlow AJ, Jones RT, McDonald AJ, Pigram PJ (2018) XPS-SurfA: an open collaborative XPS data repository using the CMSShub platform. Surf Interface Anal 50(5):527–540
33. Desnoyer AN, Bowes EG, Patrick BO, Love JA (2015) Synthesis of 2-Nickela (II) oxetanes from Nickel (0) and epoxides: structure, reactivity, and a new mechanism of formation. J Am Chem Soc 137(40):12748–12751
34. Nasrollahzadeh M, Maham M, Sajadi SM (2015) Green synthesis of CuO nanoparticles by aqueous extract of Gundelia tournefortii and evaluation of their catalytic activity for the synthesis of N-monosubstituted ureas and reduction of 4-nitrophenol. J Coll Interface Sci 455:245–253
35. Sankar R, Maheswari R, Karthik S, Shivashangari KS, Ravikumar V (2014) Anticancer activity of Ficus religiosa engineered copper oxide nanoparticles. Mater Sci Eng C 44:234–239
36. Komori H, Hashizaki R, Osaka I, Hibi T, Katano H, Taira S (2015) Nanoparticle-assisted laser desorption/ionization using sinapic acid-modified iron oxide nanoparticles for mass spectrometry analysis. Analyst 140:8134–8137
37. Masarudin MJ, Cutts SM, Evison BJ, Phillips DR, Pigram PJ (2015) Factors determining the stability, size distribution, and cellular accumulation of small, monodisperse chitosan nanoparticles

as candidate vectors for anticancer drug delivery: application to the passive encapsulation of [14C]-doxorubicin. Nanotechnol Sci Appl 8:67
38. Thakur NS, Bhaumik J, Kirar S, Banerjee UC (2017) Development of gold-based phototheranostic nanoagents through a bioinspired route and their applications in photodynamic therapy. ACS Sustain Chem Eng 5(9):7950–7960
39. Kozak DS, Sergiienko RA, Shibata E, Iizuka A, Nakamura T (2016) Non-electrolytic synthesis of copper oxide/carbon nanocomposite by surface plasma in super-dehydrated ethanol. Sci Rep 16(6):21178
40. Hua Q, Shi F, Chen K, Chang S, Ma Y, Jiang Z, Pan G, Huang W (2011) Cu_2 O-Au nanocomposites with novel structures and remarkable chemisorption capacity and photocatalytic activity. Nano Res 4(10):948–962
41. Dutta B, Kar E, Bose N, Mukherjee S (2015) Significant enhancement of the electroactive β-phase of PVDF by incorporating hydrothermally synthesized copper oxide nanoparticles. RSC Adv 5(127):105422–105434
42. Díaz-Visurraga J, Daza C, Pozo C, Becerra A, Plessing CV, García A (2012) Study on antibacterial alginate-stabilized copper nanoparticles by FT-IR and 2D-IR correlation spectroscopy. Int J Nanomed 7:3597
43. Gao D, Zhang J, Zhu J, Qi J, Zhang Z, Sui W, Shi H, Xue D (2010) Vacancy-mediated magnetism in pure copper oxide nanoparticles. Nanoscale Res Lett 5:769–772
44. Zhu J, Chen H, Liu H, Yang X, Lu L, Wang X (2004) Needle-shaped nanocrystalline CuO prepared by liquid hydrolysis of Cu $(OAc)_2$. Mater Sci Eng 384(1–2):172–176
45. Lin HH, Wang CY, Shih HC, Chen JM, Hsieh CT (2004) Characterizing well-ordered CuO nanofibrils synthesized through gas-solid reactions. J Appl Phys 95(10):5889–5895
46. Santini C, Pellei M, Gandin V, Porchia M, Tisato F, Marzano C (2013) Advances in copper complexes as anticancer agents. Chem Rev 114(1):815–862
47. Mendoza-Diaz G, Garcia-Nieto RM, Gracia-Mora I, Arias-Negrete S, Ruiz-Ramirez L, Cosenza IL, Ireta J, Moreno-Esparza R, Pannell KH, Cervantes-Lee F (1991) Synthesis, characterization and biological activity of some mixed complexes of Cu (II) and Zn (II) with antibiotics of the nalidixic acid family and N-N ligands. J Inorg Biochem 43:640
48. Teng H, Chen L (2018) Polyphenols and Bioavailability: an update. Crit Rev Food Sci Nutr. https://doi.org/10.1080/10408398.2018.1437023
49. Moses SL, Edwards VM, Brantley E (2016) Cytotoxicity in MCF-7 and MDA-MB-231 breast cancer cells, without harming MCF-10A healthy cells. Nanomed Nanotechnol 7:2
50. Levenson AS, Jordan VC (1997) MCF-7: the first hormone-responsive breast cancer cell line. Cancer Res 57:3071–3078
51. Meena R, Kumar S, Gaharwar US, Rajamani P (2017) PLGA-CTAB curcumin nanoparticles: fabrication, characterization and molecular basis of anticancer activity in triple negative breast cancer cell lines (MDA-MB-231 cells). Biomed Pharmacother 1(94):944–954
52. Kang Y, Siegel PM, Shu W, Drobnjak M, Kakonen SM, Cordón-Cardo C, Guise TA, Massagué J (2003) A multigenic program mediating breast cancer metastasis to bone. Cancer Cell 3:537–549
53. Liu H, Zhang Y, Zheng S, Weng Z, Ma J, Li Y, Xie X, Zheng W (2016) Detention of copper by sulfur nanoparticles inhibits the proliferation of A375 malignant melanoma and MCF-7 breast cancer cells. Biochem Biophys Res Commun 477(4):1031–1037
54. Laha D, Pramanik A, Maity J, Mukherjee A, Pramanik P, Laskar A, Karmakar P (2014) Interplay between autophagy and apoptosis mediated by copper oxide nanoparticles in human breast cancer cells MCF7. Biochim Biophys Acta 1840(1):1–9
55. Liou GY, Storz P (2010) Reactive oxygen species in cancer. Free Radic Res 44(5):479–496
56. Wang J, Luo B, Li X, Lu W, Yang J, Hu Y, Huang P, Wen S (2017) Inhibition of cancer growth in vitro and in vivo by a novel ROS-modulating agent with ability to eliminate stem-like cancer cells. Cell Death Dis 8(6):e2887
57. Khanna P, Ong C, Bay BH, Baeg GH (2015) Nanotoxicity: an interplay of oxidative stress, inflammation and cell death. Nanomater (Basel) 5(3):1163–1180
58. Ahamed M, Akhtar MJ, Alhadlaq HA, Alshamsan A (2016) Copper ferrite nanoparticle-induced cytotoxicity and oxidative stress in human breast cancer MCF-7 cells. Coll Surf B 142:46–54
59. Azizi M, Ghourchian H, Yazdian F, Dashtestani F, AlizadehZeinabad H (2017) Cytotoxic effect of albumin coated copper nanoparticle on human breast cancer cells of MDA-MB231. PLoS One 12(11):e0188639
60. Mukherjee S (2018) Recent progress toward antiangiogenesis application of nanomedicine in cancer therapy. Future Sci OA 4:FSO318
61. Mukherjee S, Nethi SK, Patra CR (2017) Green synthesized gold nanoparticles for future biomedical applications. In particulate technology for delivery of therapeutics. Springer, Singapore, pp 359–393
62. Setyawati MI, Leong DT (2017) Mesoporous silica nanoparticles as an antitumoral-angiogenesis strategy. ACS Appl Mater Interfaces 9(8):6690–6703
63. Gurunathan S, Lee KJ, Kalishwaralal K, Sheikpranbabu S, Vaidyanathan R, Eom SH (2009) Antiangiogenic properties of silver nanoparticles. Biomaterials 30(31):6341–6350
64. Song H, Wang W, Zhao P, Qi Z, Zhao S (2014) Cuprous oxide nanoparticles inhibit angiogenesis via downregulation of VEGFR2 expression. Nanoscale 6(6):3206–3216
65. Norton KA, Popel AS (2016) Effects of endothelial cell proliferation and migration rates in a computational model of sprouting angiogenesis. Sci Rep 6:36992
66. Trickler WJ, Lantz SM, Schrand AM, Robinson BL, Newport GD, Schlager JJ, Paule MG, Slikker W, Biris AS, Hussain SM, Ali SF (2012) Effects of copper nanoparticles on rat cerebral microvessel endothelial cells. Nanomedicine 7(6):835–846
67. Zheng W, Yang L, Liu Y, Qin X, Zhou Y, Zhou Y (2014) Liu J Mo polyoxometalate nanoparticles inhibit tumor growth and vascular endothelial growth factor induced angiogenesis. Sci Technol Adv Mater 15(3):035010

Affiliations

Desingh Raj Preeth[1] · Manickaraj Shairam[1] · Natarajan Suganya[2] · Roshandel Hootan[3] · Ravishankar Kartik[4] · Kennepohl Pierre[3] · Chatterjee Suvro[2] · Subramaniyam Rajalakshmi[1]

✉ Subramaniyam Rajalakshmi
rajimaniyam@gmail.com

[1] Chemical Biology and Nanobiotechnology Laboratory, AU-KBC Research Centre, Anna University, MIT Campus, Chromepet, Chennai 600 044, India

[2] Vascular Biology Laboratory, Department of Biotechnology and AU-KBC Research Centre, Anna University, MIT Campus, Chromepet, Chennai 600 044, India

[3] Department of Chemistry, The University of British Columbia, 2036 Main Hall, Vancouver, BC V6T 1Z1, Canada

[4] Department of Chemistry, IIT Madras, Chennai 600 036, India